


Data-Driven Damage State Assessment of RC Shear Walls with Experimental Validation

Journal Article**Author(s):**

Zhang, Hanqing; Shi, Weixing; Shan, Jiazeng; [Chatzi, Eleni](#) 

Publication date:

2023

Permanent link:

<https://doi.org/10.3929/ethz-b-000618137>

Rights / license:





[Creative Commons Attribution 4.0 International](#)

Originally published in:

Structural Control and Health Monitoring 2023, <https://doi.org/10.1155/2023/5523070>

Research Article

Data-Driven Damage State Assessment of RC Shear Walls with Experimental Validation

Hanqing Zhang ^{1,2} Weixing Shi ¹ Jiazeng Shan ^{1,3} and Eleni Chatzi ²

¹Department of Disaster Mitigation for Structures, Tongji University, Shanghai 200092, China

²Department of Civil, Environmental and Geomatic Engineering (DBAUG), ETH Zürich, Stefano-Franscini-Platz 5, Zürich 8093, Switzerland

³Shanghai Engineering Research Center for Resilient Cities and Intelligent Disaster Mitigation, Shanghai, China

Correspondence should be addressed to Jiazeng Shan; jzshan@tongji.edu.cn

Received 17 January 2023; Revised 1 April 2023; Accepted 19 April 2023; Published 1 June 2023

Academic Editor: Songye Zhu

Copyright © 2023 Hanqing Zhang et al. This is an open access article distributed under the Creative Commons Attribution License, which permits unrestricted use, distribution, and reproduction in any medium, provided the original work is properly cited.

This paper introduces a probability-based damage state evaluation methodology for shear walls deriving from a data-driven calculation. A previously proposed damage quantification index, formulated in the time domain, which is capable of tracking damage progression based on the availability of structural monitoring data, is adopted here for the quantification of structural hysteresis damages. The probability of the structure lying in a specific damage state is determined on the basis of the derived damage index and the limit state definitions, yielding valuable information for postearthquake decisions. In this study, a database of the hysteretic behavior of 1,000 shear walls, considering different structural parameters, is generated utilizing OpenSees. Four limit states of seismic performance are defined based on material properties and in relation to the simulated stress and strain data. Accordingly, the exceeding probabilities of damage can be estimated by fitting statistical models to the damage index values grouped in terms of the axial load ratio. Followingly, an informative mapping, between the monitoring-derived damage index and postearthquake damage levels, is established considering structural uncertainty. Illustrative examples, including two shear walls subjected to cyclic loading and a seven-story shear wall slice subjected to a shaking table test, are investigated to show the capability and feasibility of the proposed performance evaluation method on damage state evaluation.

1. Introduction

Reinforced concrete (RC) shear walls form the most important lateral load resisting components in high-rise buildings, dominating residential and office building construction in urban areas [1, 2]. Strong earthquake events oftentimes induce severe structural damage, including concrete cracking and crushing of structural RC members and yielding or buckling of structural steel members [3]. Such a deterioration of structural condition, which may even develop progressively under a series of seismic events, can negatively affect structural safety and compromise future performance while exposing residents and societies to significant risks of life and economic loss. An illustrative instance of such an occurrence is the collapse of an RC shear-wall building during the 2003 Bingöl earthquake [4],

while further, several RC frame-shear wall buildings experienced severe damage in the 2011 Christchurch earthquake prior to collapsing during aftershocks [5]. Under this prism, it becomes evident that a rapid and informative assessment of earthquake-excited structures can offer essential information for decision-making and provide crucial knowledge for both performance-based earthquake engineering (PBEE) and resilience-based seismic design [3, 6].

Currently, engineering demand parameters (EDPs), such as deformation, ductility, and hysteretic energy, derived on the basis of measured structural response, form the most widely adopted indicators in PBEE for characterizing and quantifying structural performance and deterioration [7], and determining damaged states according to guidelines [8]. However, the extremely limited availability of nonlinear

structural response records, as earthquakes form rare (extreme) events, constitutes a primary hurdle in the process of deriving such data-driven indicators for the safety evaluation of shear wall structures in practice [9]. In view of this, traditional visual inspection still plays an important role in the postearthquake assessment of buildings. Guidelines relying on visual inspection are developed worldwide, such as in the USA [10], Italy [11], and New Zealand [12], albeit such processes being possibly unsafe, expensive, time-consuming, and subjective even for well-trained inspectors [13, 14].

Recent advances in vibration-based structural health monitoring (SHM) techniques [15] offer a feasible solution to shift the current inspection mode to one that exploits the availability of continuously gained information on in-situ structural performance [16–19]. Such methods have been demonstrated to tackle a broad spectrum of infrastructure-related issues, including structural identification, damage detection, and quantification [20, 21]. With the utilization of the monitoring data, changes in the vibration response and physical characteristics of instrumented structures can be observed at an early damage stage [22, 23]. Correspondingly, different kinds of data-driven damage-sensitive features (DSFs) have been formulated [24], including the popular modal property-based methods [25–27] or more indirect signal processing-based methods [28–30]. On the other hand, time-domain damage identification schemes exist, on the basis of which acceleration and displacement-based damage indices (DI) [31–33] can be derived. Finally, traditional approaches, such as fitting of typical constitutive models, such as the Park–Ang model [34], have also been utilized for decades.

However, distinguished from the operational monitoring of in-service systems, one of the key challenges in SHM is the difficulty of gathering experimental or field test data from a structure in its damaged state, during which strongly nonlinear hysteretic phenomena and severe structural deterioration are experienced [35, 36]. Consequently, limited real-world demonstrations are found for data-driven damage detection in postearthquake damage assessment due to restrictions imposed from incomplete observations, linear system-based analysis algorithms, and limited records of nonlinear structural behavior [13, 37]. Currently, the determination of seismic performance levels, classified as immediate occupancy (IO), life safety (LS), and collapse prevention (CP), is still based on the qualitative criteria of typical EDPs (such as interstory drifts, inelastic element deformations, and element forces) [38], which may not fully consider the peak and cumulative damage effects. It is thus desirable to exploit data-driven monitoring methods and extend these with mappings that link the derived damage indices to damage states and performance levels. In this way, data can be harnessed to directly feed postearthquake assessment and decision support by capitalizing on knowledge from both the PBEE and SHM domains.

On the other hand, uncertainty, as an essential output of damage evaluation results, should be considered for the probabilistic evaluation of building performance under seismic loading. Uncertainty considerations lie at the core of procedures for damage and loss estimation in performance-

based earthquake engineering (PBEE) [39]. A quantification of the confidence we can allot to damage evaluation results, in place of single deterministic values, is more informative for decision-making [40]. Aligning with the seismic fragility approach, which dominates the field of PBEE, a post-earthquake assessment method adopting SHM data should yield a probabilistic evaluation of structural performance and corresponding damage states. In this respect, the DI values should be complemented with an estimate of the exceedance probabilities of specific limit states to more efficiently support postearthquake decisions.

Toward such a goal, a damage evaluation method for shear wall structures, which takes uncertainty into account, is proposed in this paper. Compared to those purely data-driven damage detection methods [41, 42], which considers uncertainty initially while proposing the method, the probabilistic metric adopted in this paper is employed directly to the calculated DI values of the shear wall components because the presented DI model is a model reference method in a data-driven manner. First, a simulated database of the hysteretic behavior of 1,000 RC shear wall components across different design parameters is generated by means of a finite element analysis. Material and section properties are utilized to define limit states and, correspondingly, determine associated damage states. The damage index (DI) values, which are calculated at each limit state for the whole database, are then used to drive seismic evaluation as an alternative form of EDPs. An informative mapping is established between the computed DI values and the determined seismic performance by clustering the data with structural design parameters and fitting the probabilistic models of the corresponding DI values. Two RC shear walls subjected to cyclic loading and a seven-story shear wall slice subjected to a shaking table test are adopted to demonstrate and validated the suggested data-driven assessment scheme.

2. Methodology

2.1. Design Framework. To evaluate structural damage under availability of SHM data, a data-driven method based on the so-called model-reference concept was previously proposed by the authors. The method relies on the availability of a reference linear system model, subjected to the same dynamic excitation, as the actual system. The associated structural damage is evaluated and further exploited for damage state classification. In this work, the previous design framework of the structural damage evaluation and seismic performance assessment is extended to consider uncertainty [43]. The specific steps to the proposed framework are outlined as follows:

- (1) The generation of a large synthetic structural response database: Over 1,000 shear wall FE models were built, based on the OpenSees platform, and was subjected to cyclic loading to extract records of structural hysteresis behavior
- (2) Critical damage state determination: The damage states in terms of seismic behavior are defined on the

basis of prescribed structural drift thresholds suggested by earthquake engineering guidelines or empirical investigations. Correspondingly, the simulated material stress and strain data were utilized to determine four key points in the hysteretic behavior, as shown in the four light blue circles in Figure 1

- (3) Damage quantification for each damage state: Damage indices reflecting the four characteristic damage states, depicted in Figure 1, were calculated on the basis of the previously proposed damage model [44] and the derived hysteresis curves. This yields a database associating damage index values to damage states for more than 1,000 data points
- (4) Exceedance probability results for each damage state: The DI results were classified into groups on the basis of shear wall design parameters. Consequently, the exceedance probabilities for each damage state, on the basis of the associated damage index values, are obtained by fitting probabilistic distribution models.

The data-driven probabilistic assessment scheme summarized in this study delivers an informative mapping between seismic performance and monitored structural damage, enabling a monitoring-based approach to structural seismic performance assessment.

2.2. Data-Driven Damage Model. The proposed method allows for derivation of structural hysteresis curves, on the basis of available SHM data, which is then exploited to quantify structural dynamic damage [45–47]. A brief introduction to and an essential description of the exploited data-driven damage model is presented below.

As inspired by the widely accepted Park–Ang model, the evaluation of the peak and cumulative damage effects is here exploited for seismic response assessment. This should be accomplished under appropriate normalization to allow for comparison. First, the peak deformation effect related to structural ductility is proposed to be computed as the minimum secant stiffness recorded during the earthquake response, which correlates to the maximum deformation point $[x_{\max}, f_{x,\max}]$. This can be determined from the monitored shear wall hysteretic behavior and is defined as

$$K_{\text{eff}} = \frac{f_{x,\max}}{x_{\max}}, \quad (1)$$

where K_{eff} is the effective stiffness, x_{\max} is the maximum deformation during the loading process and $f_{x,\max}$ is the hysteresis force corresponding to x_{\max} .

Adopting the model-reference concept described in [44], a linear system is necessarily constructed as a reference model for comparing the difference between healthy and damaged status, subjected to the same dynamic excitation. At this point, it is useful to explain that certain assumptions are here put in place in terms of monitored quantities; namely, that (i) the force at the base of the wall is measured, often approximated through a measurement of the acceleration at the top of the wall/story, (ii) that the top relative displacement is recoded, and (iii) that a measurement of the

seismic excitation is available. These quantities can be measured, although often nontrivially; however, these here serve as initiating assumptions, for proving the applicability of such a framework, which we intend to relax in future work. Theoretically, the preyield stiffness for the linear reference model of the shear wall K_{linear} can be determined by conducting linear regression for response data derived from low-amplitude forcing, when the structure behaves almost linearly. For the shear wall hysteretic behavior, the reference behavior of an assumed linear model, under the same excitation x^r , can be calculated as

$$x^r = \frac{f}{K_{\text{linear}}}, \quad (2)$$

where f denotes the structural restoring force in the hysteresis curve.

According to a previous study of the authors [47], the tracking error $[r, \dot{r}, \ddot{r}]$, which can identify the deviation of the actual structural response $[x, \dot{x}, \ddot{x}]$ to the reference (linear) response $[x^r, \dot{x}^r, \ddot{x}^r]$, has been proved capable of tracking the occurrence of structural nonlinearity and can be adopted to evaluate the cumulative damage effect. The tracking error for shear wall hysteresis behavior can be defined as

$$r = x^r - x, \quad (3)$$

where x^r and x are the reference and actual displacement response in real time, respectively.

However, the determination of K_{eff} of equation (1) is only depending on the peak displacement point, which is bound to be influenced by measurement noise and model uncertainty when using real-world data. To reflect uncertainties, an additional variable, R^2 , is computed on the basis of a hysteresis loop that contains the peak response point $[x_{\max}, f_{x,\max}]$. By performing a linear regression analysis of one such entire hysteresis loop, the value of R^2 can be determined, which offers a measure of the manifested nonlinearity and is conceptually equal to 1 for a linear model.

A data-driven index ζ for the shear-wall damage evaluation has been proposed [44] as follows:

$$\zeta = \left[\alpha_d \left(1 - \frac{K_{\text{eff}}}{K_{\text{linear}}} \right)^{R^2} + \beta_d \left(\frac{r_{\text{RMS}}}{x_{\text{RMS}}} \right)^{R^2 \cdot n_d} \right], \quad (4)$$

where K_{eff} is the effective stiffness; K_{linear} is the linear reference stiffness of the healthy structural state; R^2 is the additional linear regression statics of the peak loop; r_{RMS} is the root-mean-square (RMS) value of displacement tracking error; x_{RMS} is the RMS value of the actual displacement response; α_d , β_d and n_d are three model parameters controlling the weighting balance between the peak and cumulative damage effect with a suggested relationship of $\alpha_d + \beta_d = 1.0$. The proposed DI model can evaluate nonlinearity for any system once the hysteresis behavior can be determined.

In the authors' previous study, the proposed DI exhibits an approximately linear relationship with the reliable Park–Ang model regarding the hysteresis behavior of RC

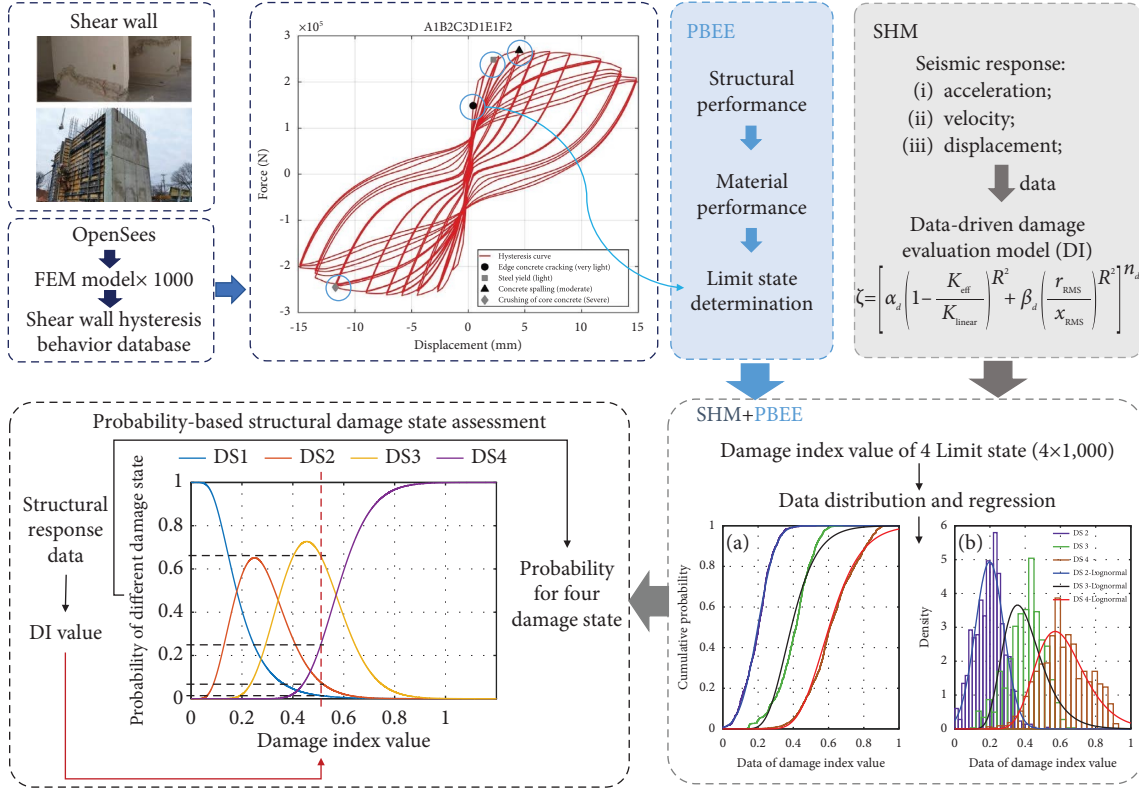


FIGURE 1: The designed framework of the proposed data-driven damage state evaluation method.

elements under the parameter set up of $\alpha_d = 0.85$, $\beta_d = 0.15$, and $n_d = 2.5$, which makes it a feasible and recommended value for potential damage evaluation for RC elements and substructures. Accordingly, this parameter setup can also be changed corresponding to different materials or failure types to balance the damage effect. Meanwhile, this model is improved in this study by substituting the RMS value of reference response with the real response x_{RMS} to assure the damage index value can converge to 1. Such improvement can bring more information for structural damage quantification and the threshold determination for shear wall components.

3. Database Generation

3.1. OpenSees Modeling. Finite element models for a large shear wall database, across numerous design parameters, have been established using the Open System for Earthquake Engineering Simulation (OpenSees) [48] for simulating the nonlinear shear wall behavior under cyclic loads. Each wall model is comprised of generic displacement beam-column elements consisting of five integration points and the widely-used fiber section model considering the shear effect, which has been shown to improve computational stability and efficiency [49]. The dispersed fiber section comprises four phases, namely unconfined concrete, confined concrete on both sides, and two longitudinal reinforcement steel bars. In terms of material constitute models, the concrete of the fiber section is endowed with the *Concrete02* OpenSees material based on the Kent and Park constitutive model [50], while

the *Steel 02* OpenSees material was adopted to model steel reinforcement based on the Menegotto and Pino model [51]. The shear walls were considered fully constrained at the bottom with a non-zero-length rotating spring and free at the top. The detailed modeling information is illustrated in Figure 2.

Prior to generating this extensive synthetic database, two experimental studies of shear walls with public data were adopted to verify the feasibility and validity of the proposed modeling scheme and eliminate the model error. More specifically, the Dazio et al. [52] and Greifenhagen and Lestuzzi [53] specimens are selected from the shear wall database of Seismic Engineering Research Infrastructures for European Synergies (SERIES) and labeled as Test 1 and 2 in this paper. Each experimental study is complete with detailed information on design, construction, testing, measurement, and availability of related reports. The fundamental information about the two adopted shear walls is summarized in Table 1. As illustrated in Figure 3, the base shear and lateral displacement curves from the OpenSees simulations sufficiently approximate the data collected from the experimental study. For Test 1, Figure 3(a) indicates that the modeling method can simulate the structural envelope curve, with exception of the approximation of the softening behavior and concrete pinching phenomena. Figure 3(b) reflects a better approximation of the structural degradation and softening behavior for Test 2. Even though no modeling approach is expected to perfectly reconstruct diverse experimental results and different approaches lead to non-identical local damages, the suggested modeling method

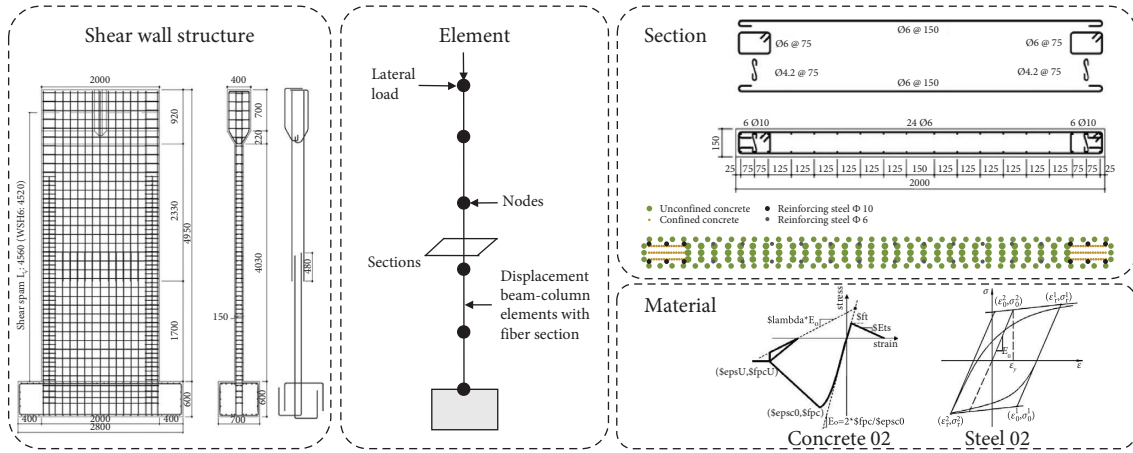


FIGURE 2: Detailed modeling information adopted for the simulated shear walls in OpenSees.

TABLE 1: Basic information of two shear walls selected from the SERIES database.

Test number	1	2
Specimen	Dazio-WSH2	Greifenhagen-M3
Sectional dimension $w \times t$ (mm)	2000 × 150	900 × 80
Height (mm)	4520	690
Concrete strength (MPa)	40.5	20.1
Longitudinal reinforcement strength (MPa)	Yield	504
	Ultimate	634
Transverse reinforcement strength (MPa)	Yield	745
	Ultimate	800
Vertical reinforcement ratio	0.30%	0.30%
Horizontal reinforcement ratio	0.25%	0.30%
Axial load ratio	0.057	0.104

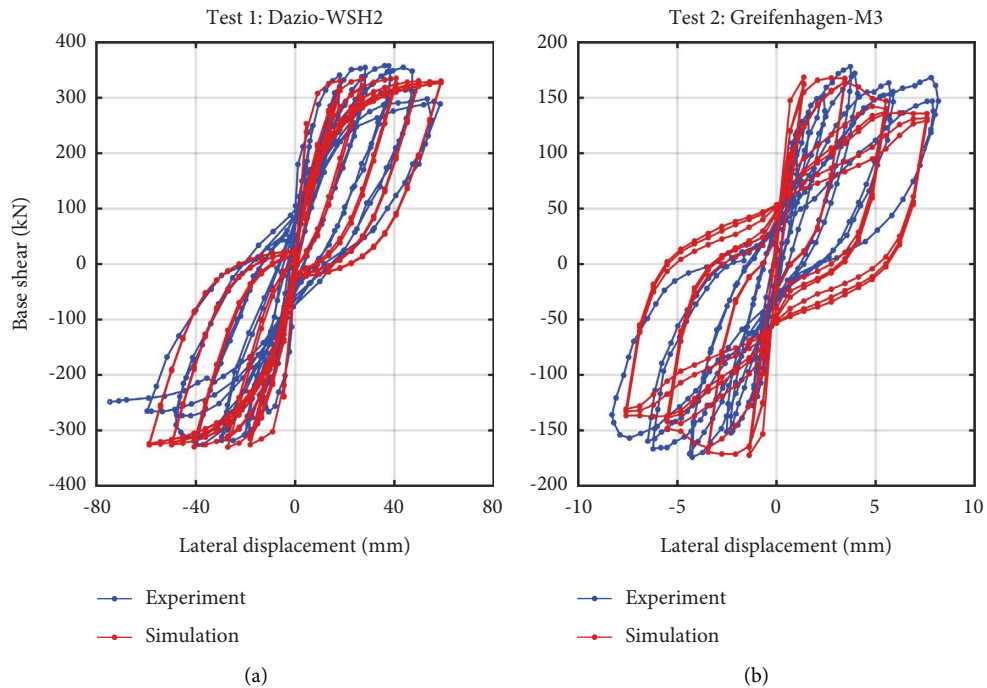


FIGURE 3: Comparison of hysteresis curves between the experiments and the OpenSees simulations for Test 1 (a) and Test 2 (b).

does prove capable in sufficiently approximating typical shear wall behavior, which will here be exploited to assess the global damage of such walls.

To generate a large-scale database of shear wall seismic behavior, 1,000 shear wall models with diverse degrading and hysteretic characteristics were numerically analyzed. Six critical design parameters of the walls were selected according to authoritative design specification [1], including the axial load ratio, span-to-depth ratio, confinement zone ratio, longitudinal reinforcement strength, transverse reinforcement strength, and transverse reinforcement interval, vary within the suggested and empirical design values, such as the axial load value ranging from 0.1 to 0.35 and the span-to-depth ratio varies from 1 to 3 [54]. A reasonably designed shear wall model can be set up with the combination of these parameters, which were classified into different groups represented by different letters (A1, A2 to E1, E2). Table 2 shows the fundamental values of each group.

3.2. Damage State Determination. The definition and classification of structural damage states (DS) according to the simulated nonlinear structural behavior is accomplished by relating the computed DIs to individual structural performance level. Four DS ranges are defined on the basis of four critical limit states (LS), motivated by the commonly adopted performance level assessment in widely used seismic guidelines [8], as illustrated in Table 3. The shear wall is assumed to exhibit no damage (DS0) prior to the appearance of cracks (DS1). When the steel bar reaches yielding (LS2), while concrete spalling does not appear (LS3), the shear wall is classified into DS2, which corresponds to the performance level of immediate occupancy (IO). Once concrete crushing appears, we assume that DS4 is reached, which requires activation of collapse prevention (CP) mechanisms.

Since the 1,000 shear wall models are synthetic, the LS determination, which is needed for labelling and classification, is straightforward according to the criteria defined in the last column of Table 3. A typical structural hysteresis curve along with the four critical LS points for each shear wall, are shown in the top-right subplot of Figure 1. Figure 4 illustrates the stiffness and strength degradation factors in terms of the reached displacement and force for each LS, which is used to determine the distributions of structural performance situations for the four defined LSs. The stiffness degradation is defined by the instantaneous stiffness at LS4 divided by the linear stiffness at LS1, while the strength degradation is defined by the ratio of the force at LS4 divided by the maximum force during the loading. Figure 4 illustrates the degradation parameters corresponding to displacement and force for four limit states. It can be found that the scatters from LS1 to LS4 can be clearly distinguished and accordingly clustered. Meanwhile, the displacement increases from LS1 to LS4, as shown in Figure 4(a), and the force increases from LS1 to LS3 and decreases at LS4, as illustrated in Figure 4(b).

3.3. Damage Quantification. The DIs computed on the basis of the simulated hysteretic curves will be utilized to subsequently evaluate the structural damage at any point during the loading process. The DI values computed by equation (4) at the interfaces between LSs can be used as thresholds to define corresponding DSs. As evidence by equation (4), the DI computation contains a peak term related to stiffness degradation and a cumulative term computed from the hysteresis time history. Figure 5 shows that the values for these two individual contributing terms and the combined DI value increase from DS1 to DS4, as expected for a measure that is to be used for quantifying seismic performance. However, as illustrated in Figures 5(a) and 5(c), outliers are noted outside the 25th and 75th percentiles (marked in the box plots), which indicates that it would be doubtful to do data processing for the whole database directly.

The previous observation can be attributed to the fact that DI results may considerably vary across the considered design parameters, which are listed in Table 2. As the axial load ratio (variable A) plays a primary role in structural damage development [55], the original dataset is grouped into six categories per axial load ratio, which are labeled as A1 to A6 in the following study; each group comprises over 150 DI values corresponding to the four defined DSs. Due to the near-zero values of DIs in DS1, which is regarded as an operational status with effectively negligible damage occurring, Figure 6 only illustrates the DI values for DS2 to DS4 for these six groups.

A significant improvement in terms of classification is illustrated in the box plot in Figure 6, fewer outliers occur, apart from some irregular DI values in DS2 under high axial ratios, as illustrated in Figure 6(a), in DS3 under moderate axial ratios, as shown in Figure 6(b), and in DS4 for low to moderate axial ratios. In addition, Figure 6(c) indicates that the DI values corresponding to DS4 are more dispersed as the ultimate near-collapse state caused by extensive deformation or multiple damage modes leads to a variability of the recorded DI values.

4. Relationship of Damage and Performance

To generate an informative mapping between performance and structural damage, the corresponding thresholds of the data-driven DIs should be determined. On the other hand, a probabilistic damage evaluation result, which quantifies confidence in the estimation, is more informative for building owners or engineers than a deterministic damage index value. We here exploit the grouped DI values at four discrete DSs to explore their statistical features and develop probabilistic models for structural performance evaluation.

4.1. Probabilistic Model Selection. First, among candidate probabilistic models, the lognormal distribution is preliminary considered because of its broad use within the earthquake engineering community for the purpose of vulnerability analysis. Figure 7(a) indicates the resulting empirical and cumulative distribution functions (CDFs) of

TABLE 2: Design parameters for configuring the shear wall database.

Variables	Definition	1	2	3	4	5	6
A	Axial load ratio	0.1	0.15	0.2	0.25	0.3	0.35
B	Span-to-depth ratio	1	1.5	2	2.5	3	
C	Ratio of confinement zone	0.15	0.2	0.25			
D	Longitudinal reinforcement strength (MPa)	503	427				
E	Transverse reinforcement strength (MPa)	425	366				
F	Transverse reinforcement interval (mm)	60	80	100			

DS2 to DS4, and the probability density functions (PDFs) along with the data distributions are shown in Figure 7(b). Generally, the lognormal distribution model can fit the CDF and PDF effectively for DS2 and DS4, including an accurate peak estimation of the PDF, and provide an acceptable evaluation for DS3.

Subsequently, the classical Kolmogorov–Smirnov test (K-S test) was utilized by setting the mean and variance of the lognormal distribution equal to the grouped DI samples to implement the goodness of fit test. Figure 8 illustrates the K-S results on group A6; the empirical and cumulative distribution functions of DS2 to DS4 are shown, accompanied by the bounds with a 95% confidence interval for the K-S test. For DS2 and DS3, all data points meet the requirements and lie within the upper and lower bound, as shown in Figures 8(a) and 8(b). However, the DI values in DS4 are unable to meet these criteria, with violation of the lower bound of the K-S test at the mid-range of the DI, as illustrated in Figure 8(c).

We wish to therefore test the efficacy of the lognormal model versus alternate statistical models. The Akaike information criterion (AIC) and the Bayesian information criterion (BIC) form popular methods for comparing the adequacy of multiple, possibly nonnested models. Figure 9 illustrates the utilization results of AIC and BIC for the six groups considering DS2 to DS4 and different commonly adopted modeling options; namely, noraml [56], lognormal [57], beta [58], gamma [59], extreme [60], generalized extreme [61], logistic [62], and Weibull [63]. It is evident that the lognormal model delivers the lowest score, which is indicated to be the optimal one, in most cases and the best overall performance among all tested statistical models. The lognormal model is thus deemed acceptable for the grouped DI database estimation.

4.2. Damage State Evaluation. By adopting the lognormal distribution model, the cumulative distribution probability can be calculated for the six groups (A1 to A6) of DI values. A conversion is subsequently carried out by subtracting the exceeding probability of two adjacent DSs to acquire a normalized probability result of lying in each DS. Ultimately, the relationship between computed DI values and the exceeding probability of DS can be determined, as illustrated in Figures 10(a)–10(f).

Figure 10(b) plots the results for group A2, corresponding to an axial ratio of 0.15. The shear wall has a 35% probability of lying in DS2 (immediately occupied) and a 65% probability of entering DS3 (limit state) when the DI value is equal to 0.4. Once the DI value increase to 0.8, the

probability of lying in DS4 (near collapse) reaches 90% with only a 10% probability of remaining in DS3 (limit state), which indicates severe structural damage to the shear wall. By contrast, Figure 10(d) illustrates that the shear wall in Group A4 is characterized by a probability of 50% of lying in DS3 and 50% of lying in DS4 for a DI value of 0.8, corresponding to the range of moderate to serious damages, respectively. Obviously, for the same damage value of 0.8, the probability of lying in DS4 has a big gap between group A2 with an axial ratio of 0.15 and group A4 with the ratio of 0.25.

These results can be used to develop a mapping between structural damage evaluation (through the computed DIs) and seismic performance levels for shear wall structures. For a rapid and practical postearthquake evaluation, the DI model can be computed, offering a quantification of the induced damage, and allowing for the corresponding exceedance probability of each discrete limit state to be determined, per Figure 10, by obtaining the basic design parameter. Then, the result containing DS levels and relevant probabilities can provide a beneficial reference for rapid postearthquake evaluation and decision-making because taking uncertainty into consideration is more practical in real-world applications.

5. Experimental Validation

5.1. Cyclic Loading Test. To investigate the application of the proposed method, the two shear walls introduced before and overviewed in Table 1 are utilized for seismic performance evaluation. Different design parameters, including the amount of boundary reinforcement, the axial force ratio, and the material properties, lead in different failure modes for the two walls. During the loading process corresponding to Test 1, flexure-shear cracks occurred with the contribution of the flexural and shear deformation. Failure is induced by fracture of the web and boundary reinforcing bars, which limit the deformation and energy dissipation performance, as illustrated in Figure 11(a). The wall in Test 2 suffered shear-related damage, with diagonal corner cracks initially observed and eventually suffering significant loss of shear capacity. The deformation capacity appears; however, not restricted, which favored ductility, as shown in Figure 12(a). The sudden concrete crushing led in termination of the test, indicating a flexural failure mode.

Once the hysteretic relationship between base shear and lateral displacement is determined, the proposed DI can be utilized to quantify structural damage. Treatment of windows of the response data over time allows tracking the DI

TABLE 3: Damage state determination corresponding to limit states and material parameters.

Damage state (range)	Performance level	Limit state (point)	Critical performance	Limit state determination in the OpenSees model
DS0	No damage	LS1	(i) Minor cracks appear on concrete covers	(i) The strain of surface concrete reaches 0.0005
DS1	Operational			
DS2	Immediate occupancy	LS2	(i) Limited yielding possibly occurs at a few locations (i) Concrete spalling (ii) Extensive damage (iii) Shear cracking	(i) The stress of longitudinal reinforcement achieves yielding stress
DS3	Life safety	LS3	(i) Crushing of core concrete (ii) Plastic hinge	(i) The strain of constrained concrete achieves cracking strain
DS4	Collapse prevention	LS4		(i) The strain of constrained concrete achieves limit strain

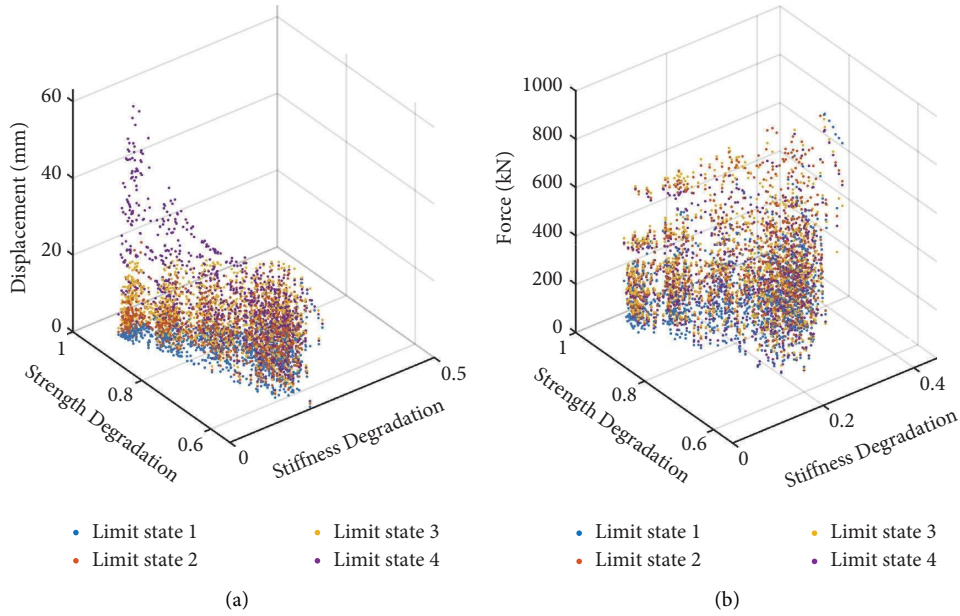


FIGURE 4: Distribution of four limit states of the database with four colored scatters regarding stiffness and strength degradation with displacement (a) and force (b).

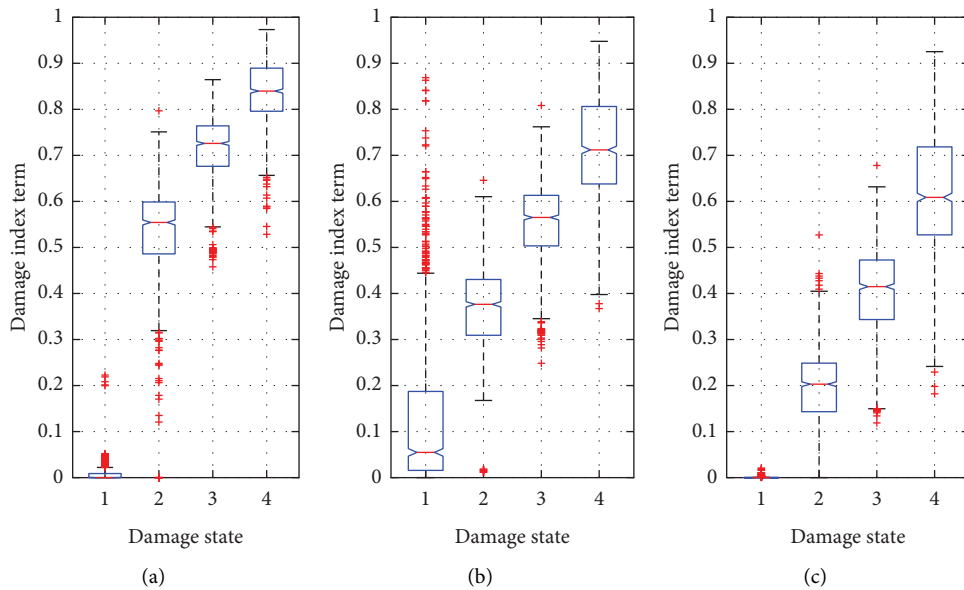


FIGURE 5: Detailed and dispersed distribution of damage index results for four critical damage states; (a) peak damage term; (b) cumulative damage term; (c) combined structural damage.

evolution over time. By adopting four DI values at different experimental stages and the information using corresponding to the shear wall axial load ratio, the exceedance probability of DS for each critical point is determined. The results are summarized in Table 4.

For the shear wall Test 1, four critical levels are determined by test observation, as shown in Figure 11(a). Figure 11(b) illustrates the developed crack and damages after failure. The time for damage development between each state from DS1 to DS3 is stable, with the DI value increasing from near zero to 0.45, as shown in Figure 11(c). With the

contribution of the confinement zone on both sides of the section, the wall shows good ductility as damage progression from DS3 to DS4 evolves over a substantial time period, reaching a DI of 0.78. After severe damage, such as core concrete crushing occurs leading to DS4, the shear wall of Test 1 fails at DI = 0.8.

Figure 12(a) shows the hysteretic behavior of the shear wall in Test 2 and Figure 12(b) illustrates the detailed failure performance after DS4. Since the shear walls have no confinement section, damage rapidly evolves from a slight to a moderate level, as shown in Figures 12(a) and 12(c). The DI

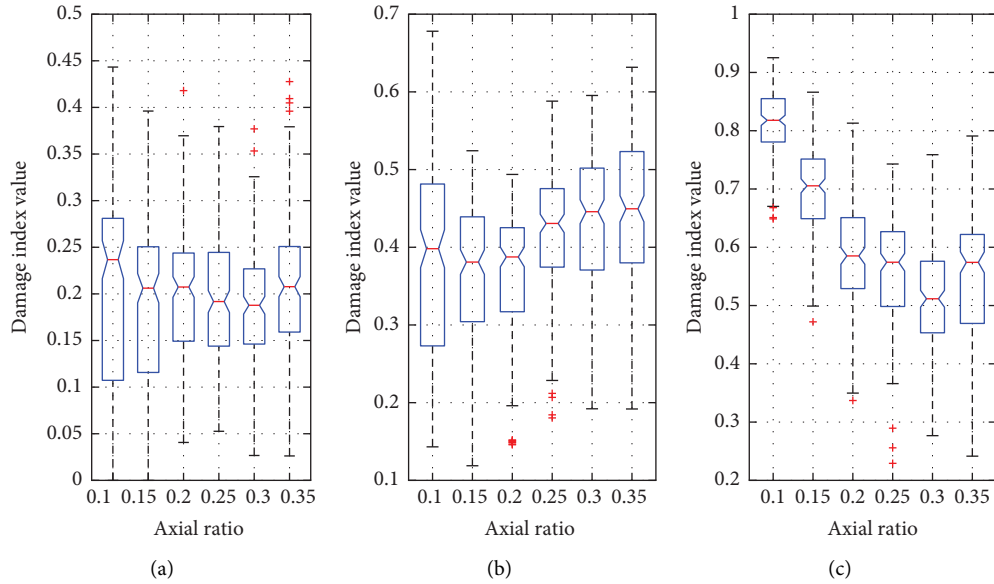


FIGURE 6: Damage index results for the three damage states after clustering by the axial ratio. (a) DS 2, (b) DS 3 and (c) DS 4.

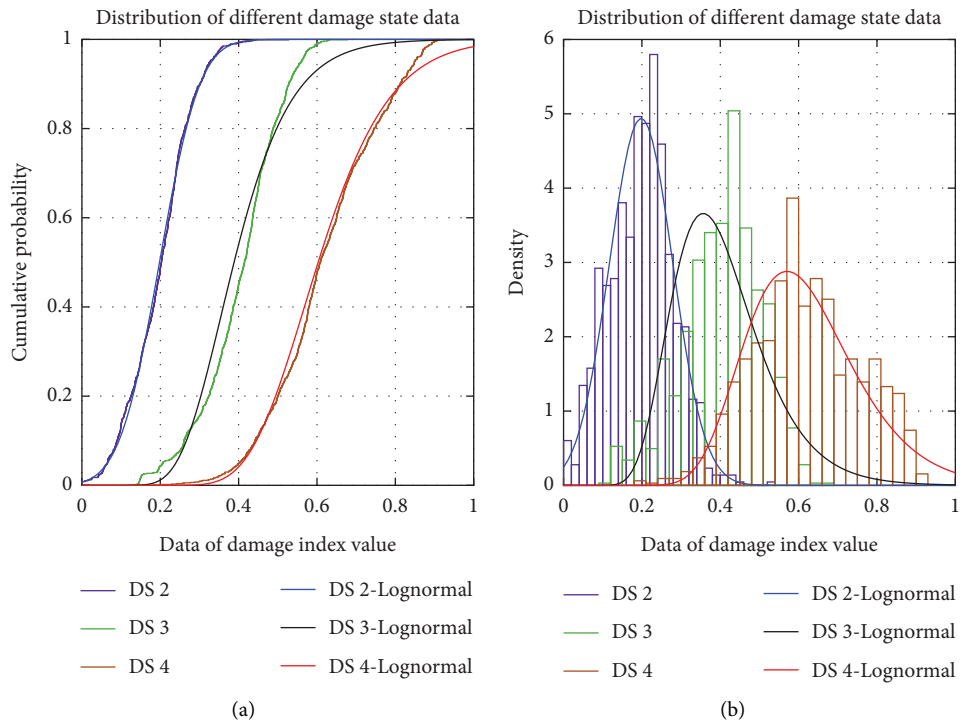


FIGURE 7: Lognormal distribution and regression of damage index values for the three damage states (a) the empirical and cumulative probability results and (b) the log-normal distribution and density results.

value is retained low during the first two states with concrete cracking and steel yielding occurring. For DS3, the damage is underestimated to some extent with a computed DI value of only 0.2 in Figure 12(c), which is not conservative in terms of damage assessment. However, the wall shows favorable ductility, which provides enough developing time from DS3 to DS4 (near collapse) with DI increasing to 1.0. The evolution of the DI value over time, shown in Figures 11(c) and

12(c), illustrates that the suggested indicator ensures adequate damage tracking performance for shear wall components.

The estimated exceedance probability results corresponding to the four states determined by experimental observation are summarized in Table 4 for two shear walls. Generally, the probability results of the shear wall in Test 1 indicate a better correlation with the four actual structural

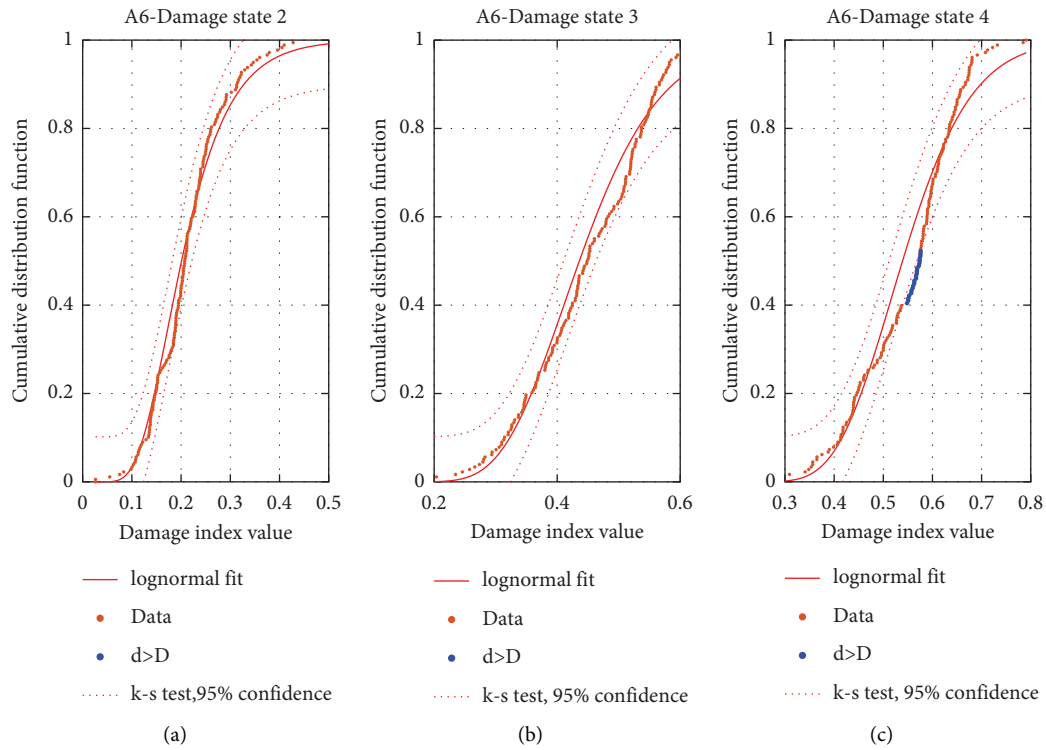


FIGURE 8: The K-S test result of the lognormal distribution for group A6: (a) A6-damage state 2; (b) A6-damage state 3; (c) A6-damage state 4.

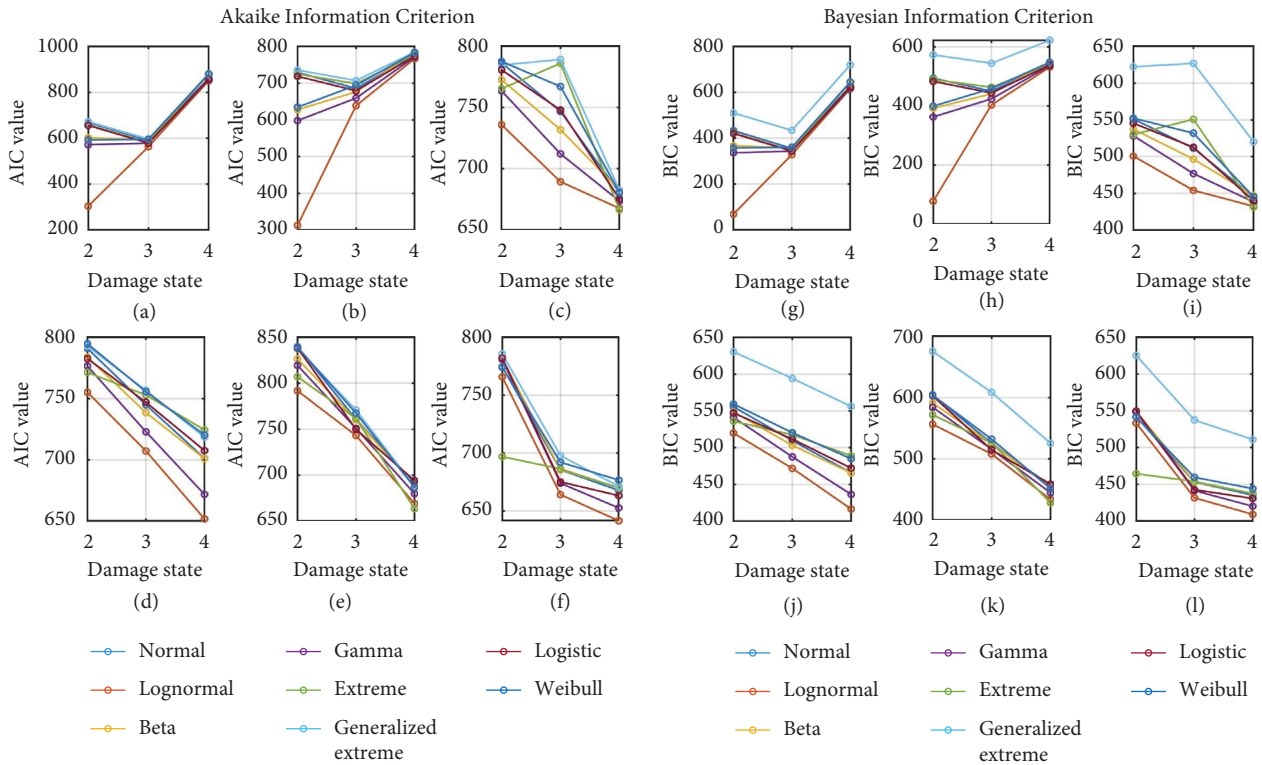


FIGURE 9: Akaike and Bayesian information criterion for different distribution models such as normal, lognormal, and beta illustrate the criterion value for each group data and the lognormal model has a lowest value.

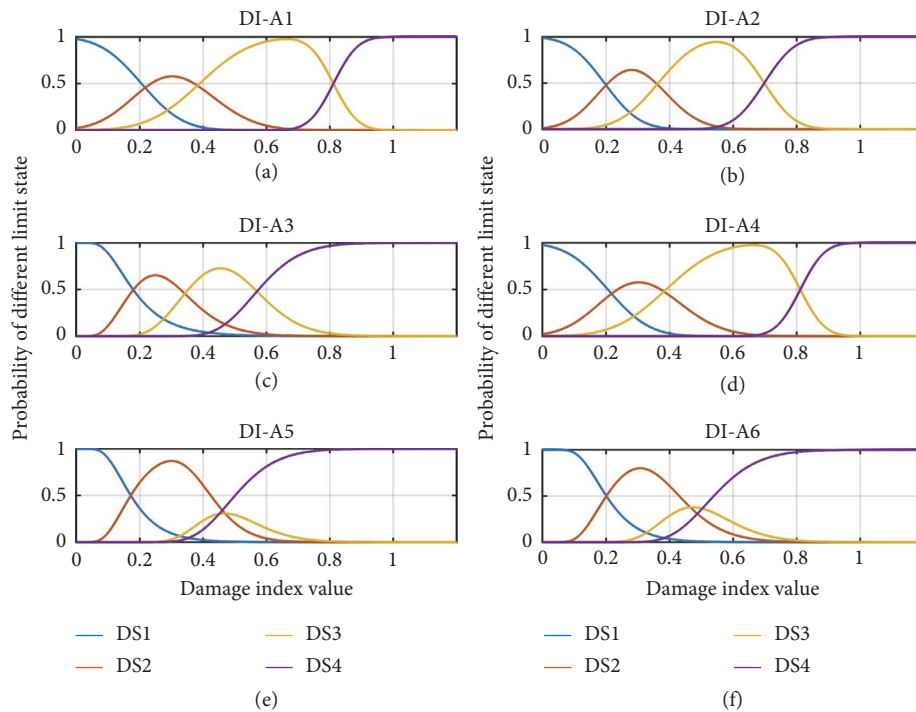


FIGURE 10: Probability-based damage state determination by using the data-driven damage index: (a) DI-A1; (b) DI-A2; (c) DI-A3; (d) DI-A4; (e) DI-A5; (f) DI-A6.

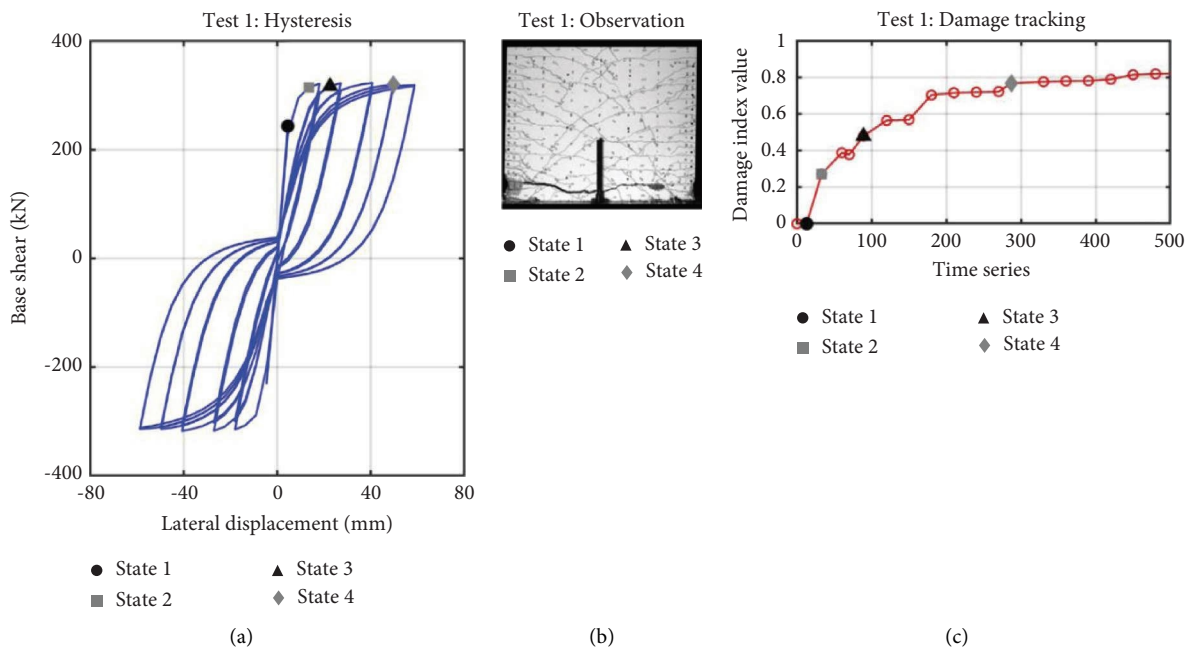


FIGURE 11: Structural hysteresis behavior, damage tracking, and state evaluation of Test 1 [52]; (a) structural hysteresis behavior and critical points; (b) experimental observation; (c) damage tracking results in time domain.

performance levels related to experimental observations. When the shear wall enters DS2, the 55% probability of entering DS2 and a 20% probability of entering DS3 are computed, indicating a margin of safety. The core concrete crushing causes the wall to enter DS4 (near collapse),

corresponding to an estimated 58% probability of entering DS3 and 42% for DS4. The overall evaluation results are conservative and thus secure for this shear wall component, and some actual serious seismic damage is overestimated by the proposed DI in some cases.

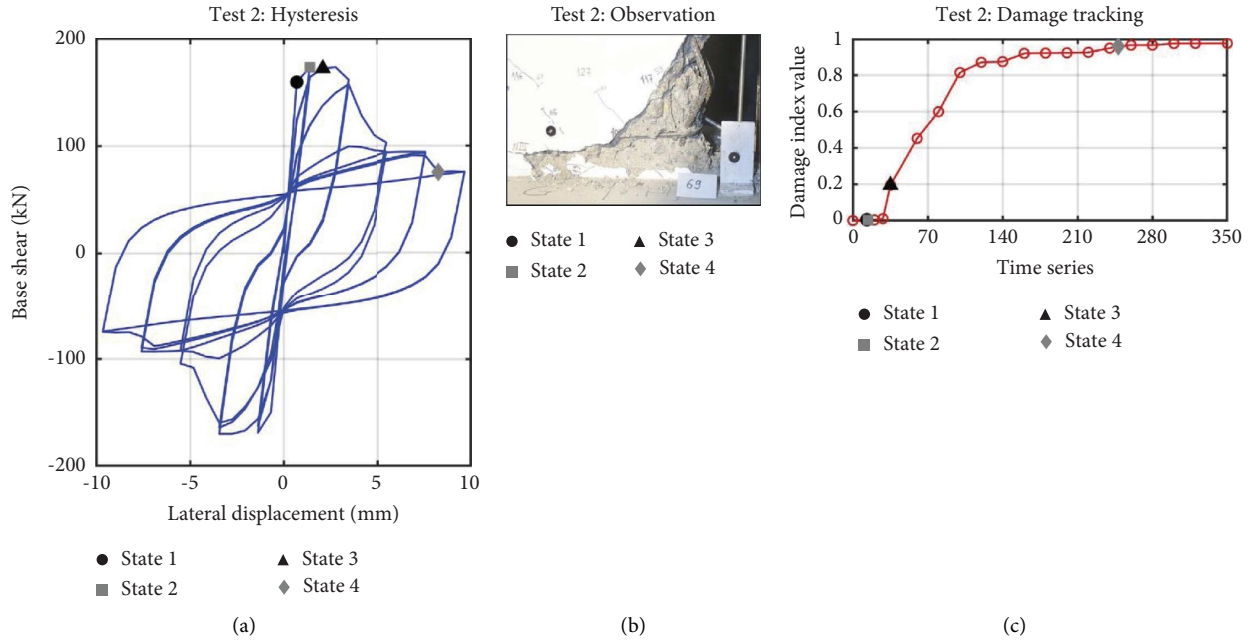


FIGURE 12: Structural hysteresis behavior, damage tracking, and state evaluation of Test 2 [53]; (a) structural hysteresis behavior and critical points; (b) experimental observation; (c) damage tracking results in time domain.

TABLE 4: Damage state probabilities for the two shear walls corresponding to four damage states.

No	Specimen	Axial load ratio	State	DI value	Probability of DS			
					DS 1 (%)	DS 2 (%)	DS 3 (%)	DS 4 (%)
1	Dazio-WSH2	0.057	1	0.0072	97.26	2.59	0.15	0.00
			2	0.2713	26.4	55.87	17.73	0.00
			3	0.4962	0.24	19.92	79.84	0.00
			4	0.7680	0.00	0.15	76.25	23.6
2	Greifenhagen-M3	0.104	1	0.0031	97.49	2.51	0.00	0.00
			2	0.0268	95.87	3.91	0.22	0.00
			3	0.1941	54.43	39.01	6.56	0.00
			4	0.9606	0.00	0.00	1.01	98.99

For Test 2, the performance level evaluation results for DS1 and DS4 fit perfectly with the actual damage observation, as both hold a 100% probability. While, for the performance level DS2 (immediately occupied) and DS3 (limit state), the proposed evaluation method results in overestimation of damage, with a low assigned probability on DS2 and only a 7% possibility allotted on entering DS3. The proposed approach seems able to warn of and prevent structural damage and provide enough margins for moderate seismic damage.

5.2. Shake Table Test. In this section, the feasibility and practical implementation of the damage state determination method with the damage evaluation model is further analyzed by adopting the shake table test of a 7-story RC shear wall slice available from DesignSafe [64]. The building was 19.2 m in height and consisted of a 3.65m-wide rectangular web wall, which provides lateral resistance along the applied direction of ground motion. The building was installed on

the shake table with a dense array of sensors, including 139 accelerometers, 88 displacement transducers, and 314 strain gauges [65]. Figure 13 illustrates the experimental setup and the structural damage observation after the sequential tests of EQ1 to EQ4, with an increasing intensity of PGAs of 0.15 g, 0.27 g, 0.35 g, and 0.91 g, respectively. The collected data was adopted for reconstructing the illustrated hysteretic curve, as shown in Figures 14(a)–14(d), and computing the associated critical EDPs for the structure. The controlling parameters of the damage model were assigned as $\alpha_d = 0.85$, $\beta_d = 0.15$, and, $n_d = 2.5$. Table 5 shows the damage quantification results when adopting the proposed damage index; these present a similar trend to the observed drift ratio and recorded concrete strain, which increase from EQ1 to EQ4 correlates to a developing structural damage.

The axial ratio should first be determined with geometric and loading information to determine the probability for each damage state. The structure herein can be classified into group A1, with a calculated axial load ratio of 0.1007. Subsequently, the calculated DI values in Table 5 and the

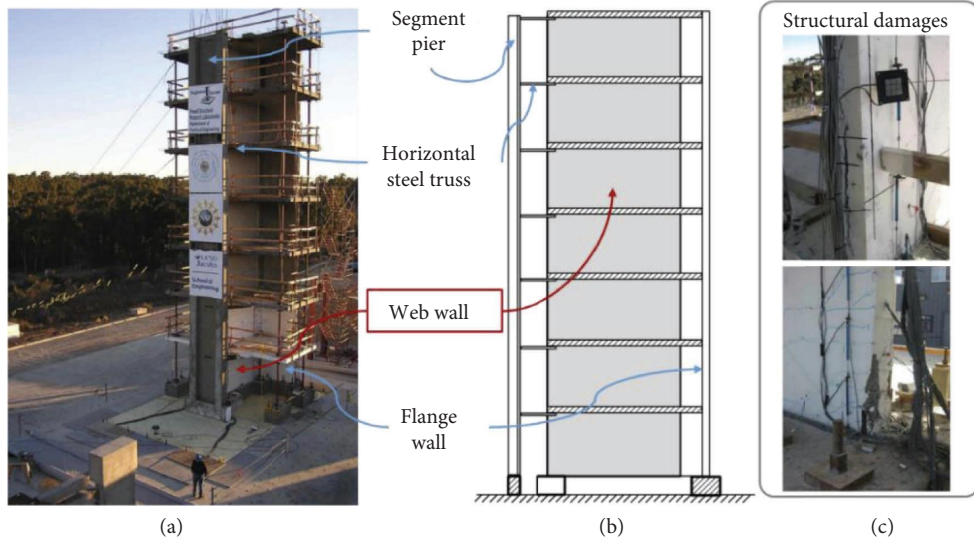


FIGURE 13: Shake table test of a seven-story RC shear wall building under four earthquake cases [65]: (a) experimental setup; (b) system illustration; (c) observed structural damages after all the cases.

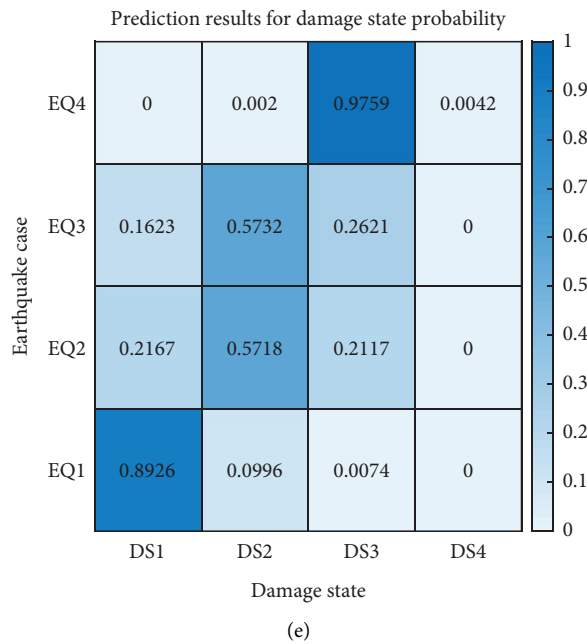
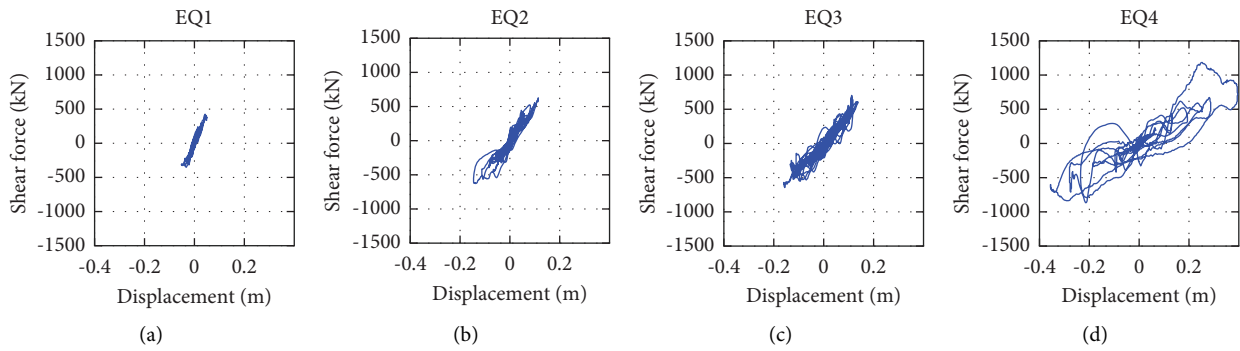


FIGURE 14: Damage state possibility results with hysteresis behaviors for four earthquake cases.

TABLE 5: Structural damage evaluation result and critical EDPs for four earthquake cases.

Case	Damage index value	Interstory drift ratio (%)	Roof drift ratio (%)	Roof residual displacements (mm)	Concrete compressive strain (%)
EQ1	0.0779	0.35	0.28	5.6	-0.07
EQ2	0.2864	0.89	0.75	4.3	-0.17
EQ3	0.3073	1.03	0.83	4.3	-0.18
EQ4	0.6520	2.36	2.06	15.5	-0.39

relationship from Figure 10(a) can be adopted to determine the structural damage state under four earthquake cases. The heatmap shown in Figure 14(e) shows the relationship between the development of structural damage states and the increasingly excitation from EQ1 to EQ4. As illustrated, for the case of EQ1 corresponding to a low-amplitude excitation, the shear wall structure is attributed a probability of 89.3% to stay within DS1. In terms of EQ2 and EQ3, the major damage state is evaluated as DS2 with a probability of around 0.57; however, the EQ3 presents a larger probability for DS3. For the most severe earthquake case (EQ4), the result assigns a 97.58% possibility for DS3, which matches well with the structural damage development and the experimental observations such as concrete spalling and bar yielding, as well as the structural hysteresis behavior. Promisingly, the damage quantification and state probability determination methods interpret the dynamic monitoring data deeply with a clear correlation to the seismic evaluation, regarding the inherent structural uncertainty under non-stationary excitations.

6. Conclusion

A probability-based damage assessment method for shear walls is presented in this paper to determine the structural damage states by adopting a previously proposed data-driven damage tracking index. Four major steps are described in the proposed the methodological framework for seismic assessment: (1) the database generation of target structural behavior; (2) critical damage state determination; (3) data-driven damage quantification; and (4) database-based statistical mapping establishment between structural damage and seismic performance.

The structural hysteretic behavior database is first generated to derive and express mechanical knowledge of the target structural behavior. Numerical simulations for over 1,000 RC shear walls are performed by means of a FE analysis to extract the resulting hysteresis behavior and support the classification of critical DSs. The suggested monitoring-based DI can be utilized to quantify the structural damage at four critical LSs for each shear wall. By fitting the lognormal model on the grouped data divided by the axial load ratio, the exceedance probabilities of DSs corresponding to DI values can be established. The regressed results can be regarded as thresholds of the DI value corresponding to seismic performances considering structural uncertainty.

Two RC shear walls subjected to cyclic loading and a seven-story shear wall slice, subjected to a shaking table test, are adopted as component-level and system-level

experimental studies, respectively, to demonstrate the practical capability of the proposed method. The DI model can accurately track and evaluate the structural damage development over time, with a favorable correlation with the actual hysteretic behavior and experimental observation. The DS and the exceedance probabilities, corresponding to four specified structural damage levels can be further determined by means of the presented structural performance evaluation method.

This study presents a valuable structural seismic performance evaluation method for shear wall structures, resulting in an assessment of the probability that the structure enters a specific DS. Such an informative mapping between structural monitoring data and performance level offers valuable knowledge for rapid postearthquake evaluation and decision-making, which would be beneficial for structural recovery and resilience. Noticeably, the proposed method can be adapted to the structural or substructural level once the hysteresis behavior can be obtained, which demonstrates strong application capabilities.

Despite the good evaluation performance, limitations remain to be addressed and need further investigation in future research, such as the parameter selection method for the DI model. Future work will focus on (1) the utilization of system identification and response estimation methods to perform story-level damage evaluation; (2) the extension of the current method to account for diversified structural failure types, such as shear-flexure coupling and further expansion to different structural types, such as bridges and steel structures; and (3) the clarification of uncertainty factors and the corresponding effect, such as model error.

Data Availability

Some or all of the data, models, or code that support the findings of this study are available from the corresponding author upon reasonable request

Conflicts of Interest

The authors declare that they have no conflicts of interest.

Acknowledgments

This study was sponsored by the National Natural Science Foundation of China (Grant nos: 51878483 and 52278312), the Shanghai Rising-Star program (Grant no. 20QC1400700), the Shanghai Qi Zhi Institute (Grant no. SYXF0120020109), the Peak Discipline Construction Project of Shanghai (No. 2021-CE-03), and the Shanghai Municipal Science and Technology Major Project (2021SHZDZX0100).

References

- [1] C. Xiong, X. Lu, and X. Lin, "Damage assessment of shear wall components for RC frame-shear wall buildings using story curvature as engineering demand parameter," *Engineering Structures*, vol. 189, pp. 77–88, 2019.
- [2] D. R. Pant, M. Montgomery, and C. Christopoulos, "Analytical study on the dynamic properties of viscoelastically coupled shear walls in high-rise buildings," *Journal of Engineering Mechanics*, vol. 143, no. 8, Article ID 04017047, 2017.
- [3] K. Erazo, B. Moaveni, and S. Nagarajaiah, "Bayesian seismic strong-motion response and damage estimation with application to a full-scale seven story shear wall structure," *Engineering Structures*, vol. 186, pp. 146–160, 2019.
- [4] Ö. Çavdar, A. Çavdar, and E. Bayraktar, "Earthquake performance of reinforced-concrete shear-wall structure using nonlinear methods," *Journal of Performance of Constructed Facilities*, vol. 32, no. 1, Article ID 04017122, 2018.
- [5] A. Kaiser, C. Holden, J. Beavan et al., "The Mw 6.2 Christchurch earthquake of February 2011: preliminary report," *New Zealand Journal of Geology and Geophysics*, vol. 55, no. 1, pp. 67–90, 2012.
- [6] M. Chaabane, M. Mansouri, A. Ben Hamida, H. Nounou, and M. Nounou, "Multivariate statistical process control-based hypothesis testing for damage detection in structural health monitoring systems," *Structural Control and Health Monitoring*, vol. 26, no. 1, Article ID e2287, 2019.
- [7] I. Iervolino, "Assessing uncertainty in estimation of seismic response for PBEE," *Earthquake Engineering & Structural Dynamics*, vol. 46, no. 10, pp. 1711–1723, 2017.
- [8] Fema, *Seismic Performance Assessment of Buildings*, FEMA, Washington, D.C, USA, 2018.
- [9] C. Zhang, Z. Alam, L. Sun, Z. Su, and B. Samali, "Fibre Bragg grating sensor-based damage response monitoring of an asymmetric reinforced concrete shear wall structure subjected to progressive seismic loads," *Structural Control and Health Monitoring*, vol. 26, no. 3, Article ID e2307, 2019.
- [10] C. Rojahn, C. D. Poland, and C. Scawthorn, "Rapid visual screening of buildings for potential seismic hazards: a handbook," *Applied Technology Council*, vol. 21, 1988.
- [11] C. Baggio, A. Bernardini, and R. Colozza, "Field manual for post-earthquake damage and safety assessment and short term countermeasures (AeDES)," *European commission—joint research centre—institute for the protection and security of the citizen*, *EUR*, vol. 22868, 2007.
- [12] J. D. Marshall, K. Jaiswal, N. Gould, F. Turner, B. Lizundia, and J. C. Barnes, "Post-earthquake building safety inspection: lessons from the canterbury, New Zealand, earthquakes," *Earthquake Spectra*, vol. 29, no. 3, pp. 1091–1107, 2013.
- [13] L. Sun, Z. Shang, Y. Xia, S. Bhowmick, and S. Nagarajaiah, "Review of bridge structural health monitoring aided by big data and artificial intelligence: from condition assessment to damage detection," *Journal of Structural Engineering*, vol. 146, no. 5, Article ID 04020073, 2020.
- [14] G. De Martino, M. Di Ludovico, A. Prota, C. Moroni, G. Manfredi, and M. Dolce, "Estimation of repair costs for RC and masonry residential buildings based on damage data collected by post-earthquake visual inspection," *Bulletin of Earthquake Engineering*, vol. 15, no. 4, pp. 1681–1706, 2017.
- [15] M. P. Limongelli, E. Chatzi, M. Döhler, G. Lombaert, and E. Reynders, "Towards extraction of vibration-based damage indicators," in *EWSHM-8th European Workshop on Structural Health Monitoring*, Bilbao, Spain, 2016.
- [16] J. Ou and H. Li, "Structural health monitoring in mainland China: review and future trends," *Structural Health Monitoring*, vol. 9, no. 3, pp. 219–231, 2010.
- [17] P. F. Giordano, C. Iacovino, S. Quqa, and M. P. Limongelli, "The value of seismic structural health monitoring for post-earthquake building evacuation," *Bulletin of Earthquake Engineering*, 2022.
- [18] B. K. Oh, S. H. Lee, and H. S. Park, "Damage localization method for building structures based on the interrelation of dynamic displacement measurements using convolutional neural network," *Structural Control and Health Monitoring*, vol. 27, no. 8, Article ID e2578, 2020.
- [19] Y. Bao, Z. Tang, H. Li, and Y. Zhang, "Computer vision and deep learning-based data anomaly detection method for structural health monitoring," *Structural Health Monitoring*, vol. 18, no. 2, pp. 401–421, 2019.
- [20] M. N. Chatzis, E. N. Chatzi, and A. W. Smyth, "On the observability and identifiability of nonlinear structural and mechanical systems," *Structural Control and Health Monitoring*, vol. 22, no. 3, pp. 574–593, 2015.
- [21] M. M. R. Taha, A. Noureldin, J. L. Lucero, and T. J. Baca, "Wavelet transform for structural health monitoring: a compendium of uses and features," *Structural Health Monitoring*, vol. 5, no. 3, pp. 267–295, 2006.
- [22] Y. Lei, F. Chen, and H. Zhou, "An algorithm based on two-step Kalman filter for intelligent structural damage detection," *Structural Control and Health Monitoring*, vol. 22, no. 4, pp. 694–706, 2015.
- [23] A. A. Mousavi, C. Zhang, S. F. Masri, and G. Gholipour, "Damage detection and characterization of a scaled model steel truss bridge using combined complete ensemble empirical mode decomposition with adaptive noise and multiple signal classification approach," *Structural Health Monitoring*, vol. 21, no. 4, pp. 1833–1848, 2022.
- [24] R. Hou and Y. Xia, "Review on the new development of vibration-based damage identification for civil engineering structures: 2010–2019," *Journal of Sound and Vibration*, vol. 491, Article ID 115741, 2021.
- [25] M. Radziński, M. Krawczuk, and M. Palacz, "Improvement of damage detection methods based on experimental modal parameters," *Mechanical Systems and Signal Processing*, vol. 25, no. 6, pp. 2169–2190, 2011.
- [26] Z. Nie, H. Hao, and H. Ma, "Using vibration phase space topology changes for structural damage detection," *Structural Health Monitoring*, vol. 11, no. 5, pp. 538–557, 2012.
- [27] Y. Shokrani, V. K. Dertimanis, E. N. Chatzi, and M. Savoia, "On the use of mode shape curvatures for damage localization under varying environmental conditions," *Structural Control and Health Monitoring*, vol. 25, no. 4, Article ID e2132, 2018.
- [28] Y. Yang and S. Nagarajaiah, "Blind identification of damage in time-varying systems using independent component analysis with wavelet transform," *Mechanical Systems and Signal Processing*, vol. 47, no. 1–2, pp. 3–20, 2014.
- [29] J. Mao, H. Wang, and B. F. Spencer, "Toward data anomaly detection for automated structural health monitoring: exploiting generative adversarial nets and autoencoders," *Structural Health Monitoring*, vol. 20, no. 4, pp. 1609–1626, 2021.
- [30] Y. An, E. Chatzi, S.-H. Sim, S. Laflamme, B. Blachowski, and J. Ou, "Recent progress and future trends on damage identification methods for bridge structures," *Structural Control and Health Monitoring*, vol. 26, no. 10, Article ID e2416, 2019.

- [31] Y. An, B. Blachowski, and J. Ou, "A degree of dispersion-based damage localization method," *Structural Control and Health Monitoring*, vol. 23, no. 1, pp. 176–192, 2016.
- [32] S. Wernitz, E. Chatzi, B. Hofmeister, M. Wolniak, W. Shen, and R. Rolfes, "On noise covariance estimation for Kalman filter-based damage localization," *Mechanical Systems and Signal Processing*, vol. 170, Article ID 108808, 2022.
- [33] M. N. Chatzis, E. N. Chatzi, and A. W. Smyth, "An experimental validation of time domain system identification methods with fusion of heterogeneous data," *Earthquake Engineering & Structural Dynamics*, vol. 44, no. 4, pp. 523–547, 2015.
- [34] Y. J. Park and A. H. S. Ang, "Mechanistic seismic damage model for reinforced concrete," *Journal of Structural Engineering*, vol. 111, no. 4, pp. 722–739, 1985.
- [35] R. J. Barthorpe, A. J. Hughes, and P. Gardner, "A forward model driven structural health monitoring paradigm: damage detection," *Model Validation and Uncertainty Quantification*, vol. 3, 2022.
- [36] M.-L. Wang and S. P. Shah, "Reinforced concrete hysteresis model based on the damage concept," *Earthquake Engineering & Structural Dynamics*, vol. 15, no. 8, pp. 993–1003, 1987.
- [37] M. Roohi and E. M. Hernandez, "Performance-based post-earthquake decision making for instrumented buildings," *Journal of Civil Structural Health Monitoring*, vol. 10, no. 5, pp. 775–792, 2020.
- [38] FEMA, *Prestandard and Commentary for the Seismic Rehabilitation of Buildings*, FEMA, Washington, DC, USA, 2000.
- [39] T.-H. Lee and K. M. Mosalam, "Seismic demand sensitivity of reinforced concrete shear-wall building using FOSM method," *Earthquake Engineering & Structural Dynamics*, vol. 34, no. 14, pp. 1719–1736, 2005.
- [40] S. O. Sajedi and X. Liang, "Uncertainty-assisted deep vision structural health monitoring," *Computer-Aided Civil and Infrastructure Engineering*, vol. 36, no. 2, pp. 126–142, 2021.
- [41] W.-J. Yan, D. Chronopoulos, K.-V. Yuen, and Y. C. Zhu, "Structural anomaly detection based on probabilistic distance measures of transmissibility function and statistical threshold selection scheme," *Mechanical Systems and Signal Processing*, vol. 162, Article ID 108009, 2022.
- [42] L.-F. Mei, W.-J. Yan, K.-V. Yuen, and M. Beer, "Structural novelty detection with Laplace asymptotic expansion of the Bhattacharyya distance of transmissibility and Bayesian resampling scheme," *Journal of Sound and Vibration*, vol. 540, Article ID 117277, 2022.
- [43] J. Shan, Y. Gong, J. Liu, W. Shi, and H. Zhang, "Damage tracking and evaluation of RC columns with structural performances by using seismic monitoring data," *Bulletin of Earthquake Engineering*, vol. 20, no. 9, pp. 4561–4587, 2022.
- [44] J. Shan, H. Zhang, Y. Ouyang, and W. Shi, "Data-driven damage tracking and hysteresis evaluation of earthquake-excited structures with test validation," *Engineering Structures*, vol. 207, Article ID 110214, 2020.
- [45] E. Poskus, G. W. Rodgers, C. Zhou, and J. G. Chase, "Damage identification for hysteretic structures using a mode decomposition method," *Computer-Aided Civil and Infrastructure Engineering*, vol. 33, no. 2, pp. 97–109, 2018.
- [46] L. Wang, J. Guo, and I. Takewaki, "Real-time hysteresis identification in structures based on restoring force reconstruction and Kalman filter," *Mechanical Systems and Signal Processing*, vol. 150, Article ID 107297, 2021.
- [47] J. Shan, Y. Ouyang, H. Zhang, and W. Shi, "Model-reference damage tracking and evaluation of hysteretic structures with test validation," *Mechanical Systems and Signal Processing*, vol. 118, pp. 443–460, 2019.
- [48] S. Mazzoni, F. McKenna, and M. H. Scott, "OpenSees command language manual," *Pacific earthquake engineering research (PEER) center*, vol. 264, 2006.
- [49] P. Martinelli and F. C. Filippou, "Simulation of the shaking table test of a seven-story shear wall building," *Earthquake Engineering & Structural Dynamics*, vol. 38, no. 5, pp. 587–607, 2009.
- [50] D. C. Kent and R. Park, "Flexural members with confined concrete," *Journal of the Structural Division*, vol. 97, no. 7, pp. 1969–1990, 1971.
- [51] M. Menegotto and P. E. Pinto, "Slender RC compressed members in biaxial bending," *Journal of the Structural Division*, vol. 103, no. 3, pp. 587–605, 1977.
- [52] A. Dazio, K. Beyer, and H. Bachmann, "Quasi-static cyclic tests and plastic hinge analysis of RC structural walls," *Engineering Structures*, vol. 31, no. 7, pp. 1556–1571, 2009.
- [53] C. Greifenhagen and P. Lestuzzi, "Static cyclic tests on lightly reinforced concrete shear walls," *Engineering Structures*, vol. 27, no. 11, pp. 1703–1712, 2005.
- [54] S. Mangalathu, H. Jang, S.-H. Hwang, and J. S. Jeon, "Data-driven machine-learning-based seismic failure mode identification of reinforced concrete shear walls," *Engineering Structures*, vol. 208, Article ID 110331, 2020.
- [55] J. W. Wallace, "New methodology for seismic design of RC shear walls," *Journal of Structural Engineering*, vol. 120, no. 3, pp. 863–884, 1994.
- [56] D. G. Altman and J. M. Bland, "Statistics notes: the normal distribution," *BMJ*, vol. 310, no. 6975, p. 298, 1995.
- [57] E. L. Crow and K. Shimizu, *Lognormal Distributions*, Marcel Dekker, New York, NY, USA, 1987.
- [58] A. K. Gupta and S. Nadarajah, *Handbook of Beta Distribution and its Applications*, CRC Press, Boca Raton, FL, USA, 2004.
- [59] E. W. Stacy, "A generalization of the gamma distribution," *The Annals of Mathematical Statistics*, vol. 33, no. 3, pp. 1187–1192, 1962.
- [60] A. L. Dekkers, J. H. Einmahl, and L. De Haan, "A moment estimator for the index of an extreme-value distribution," *Annals of Statistics*, pp. 1833–1855, 1989.
- [61] J. R. M. Hosking, J. R. Wallis, and E. F. Wood, "Estimation of the generalized extreme-value distribution by the method of probability-weighted moments," *Technometrics*, vol. 27, no. 3, pp. 251–261, 1985.
- [62] N. Balakrishnan, *Handbook of the Logistic Distribution*, CRC Press, Boca Raton, FL, USA, 2013.
- [63] H. Rinne, *The Weibull Distribution: A Handbook*, Chapman and Hall/CRC, Boca Raton, FL, USA, 2008.
- [64] M. Panagiotou, J. Restrepo, and J. Conte, "Shake table test of 7-story RC bearing wall building," *Design and Culture*, 2006.
- [65] M. Panagiotou and J. I. Restrepo, "Displacement-based method of analysis for regular reinforced-concrete wall buildings: application to a full-scale 7-story building slice tested at UC-san diego," *Journal of Structural Engineering*, vol. 137, no. 6, pp. 677–690, 2011.